Supporting Online Material for

Broadband Invisibility by Non-Euclidean Cloaking

Ulf Leonhardt* and Tomás Tyc

*To whom correspondence should be addressed. E-mail: ulf@st-andrews.ac.uk

Published 20 November 2008 on *Science* Express
DOI: 10.1126/science.1166332

This PDF file includes:

Broadband Invisibility by Non-Euclidean Cloaking: Supporting Online Material

Ulf Leonhardt[1,2*] and Tomáš Tyc[2,3]

[1]Physics Department, National University of Singapore,
2 Science Drive 3, Singapore 117542, Singapore

[2]School of Physics and Astronomy,
University of St Andrews, North Haugh, St Andrews, KY16 9SS, UK

[3]Institute of Theoretical Physics and Astrophysics,
Masaryk University, Kotlarska 2, 61137 Brno, Czech Republic

[*]To whom correspondence should be addressed; E-mail: ulf@st-andrews.ac.uk.

In this supplement to our paper we describe our calculations in detail. We also explain some of the theoretical background behind non-Euclidean cloaking.

Geometry and media

Our starting point is the relationship between dielectric materials, including metamaterials, and the geometry of space (*S1*). We are very brief here – the reader is referred to the article (*S1*) for a self-contained primer on the subject. Consider an anisotropic linear medium with electric permittivity tensor ε^{ij} and magnetic permeability μ^{ij}. We assume that the medium is impedance-matched to the vacuum [but in practice this requirement might be relaxed (*S2, S3*)],

$$\varepsilon^{ij} = \mu^{ij} \ . \tag{S1}$$

The material acts as a spatial geometry with metric tensor g_{ij} (*S1*). Specifically, the inverse matrix of the metric tensor, g^{ij}, is given by

$$g^{ij} = \frac{\varepsilon^{ij}}{\det \varepsilon} \tag{S2}$$

where $\det \varepsilon$ denotes the determinant of ε^{ij}. A dielectric medium acts as a geometry for electromagnetic fields, but a geometry appears as a medium as well, because, by inversion of relationship (S2),

$$\varepsilon^{ij} = \sqrt{g}\, g^{ij} \tag{S3}$$

where g is the determinant of g_{ij}. From an engineering perspective, Eqs. (S1) and (S3) describe the material properties required to implement the geometry g_{ij}, for example a geometry that is suitable for cloaking. Note that so far we have assumed that ε^{ij} is given in Cartesian coordinates. The geometry g_{ij} is an effective geometry for the electromagnetic field that differs from the Cartesian background, but we have described it by a matrix in Cartesian coordinates. In many cases, however, it is advantageous to employ coordinate systems that are adapted to the geometrical shape and profile of the material. For instance, we will use variations of bipolar coordinates for our examples of non-Euclidean cloaking devices. We denote the metric tensor of the background coordinate system by γ_{ij} with the determinant γ. In this case (*S1, S4*)

$$\varepsilon^{ij} = \frac{\sqrt{g}}{\sqrt{\gamma}}\, g^{ij} \ . \tag{S4}$$

A particularly convenient quantity is the mixed tensor

$$\varepsilon^{i}{}_{j} = \varepsilon^{ik}\, \gamma_{kj} \, . \tag{S5}$$

Here, and throughout this and the next section we employ Einstein's summation convention over repeated upper and lower indices; $\varepsilon^{ik}\, \gamma_{kj}$ thus abbreviates the sum $\sum_k \varepsilon^{ik}\, \gamma_{kj}$. The mixed tensor $\varepsilon^{i}{}_{j}$ is convenient, because the eigenvalues of $\varepsilon^{i}{}_{j}$ are invariant under coordinate transformations (*S1*), in particular under a transformation to Cartesian coordinates. Consequently, we can read off the eigenvalues of the dielectric properties from the eigenvalues of $\varepsilon^{i}{}_{j}$. Moreover, if $\varepsilon^{i}{}_{j}$ is diagonal the coordinate lines of the background system define the principal axes of the material. These features of the mixed permittivity tensor frequently save tedious calculations.

Transformation media and geometrical optics

In a given spatial geometry or, equivalently, in an impedance-matched material, the electric field strength components E_i obey the wave equation (*S1*)

$$\nabla^j \nabla_j\, E_i + R_{ij}\, g^{jk}\, E_k + \frac{\omega^2}{c^2}\, E_i = 0 \tag{S6}$$

for frequencies ω, and they satisfy the transversality condition

$$\nabla^i\, E_i = 0 \ . \tag{S7}$$

As usual, c denotes the speed of light in vacuum, ∇_i and ∇^i are covariant derivatives (*S1*) with respect to the geometry g_{ij} and R_{ij} is the Ricci tensor, the contracted Riemann curvature tensor $R^{i}{}_{jkl}$,

$$R_{ij} = R^{k}{}_{ijk} \ . \tag{S8}$$

The Riemann tensor is given by

$$R^i{}_{jkl} = \frac{\partial \Gamma^i{}_{jl}}{\partial x^k} - \frac{\partial \Gamma^i{}_{jk}}{\partial x^l} + \Gamma^i{}_{mk}\Gamma^m_{jl} - \Gamma^i{}_{ml}\Gamma^m_{jk} \tag{S9}$$

in terms of the Christoffel symbols

$$\Gamma^i{}_{jk} = \frac{1}{2} g^{il} \left(\frac{\partial g_{lj}}{\partial x^k} + \frac{\partial g_{lk}}{\partial x^j} - \frac{\partial g_{jk}}{\partial x^l} \right) . \tag{S10}$$

Transformation media are materials that implement coordinate transformations from physical space to a virtual empty space, electromagnetic space. They are the materials of perfect invisibility devices (*S5*), but also for perfect lenses (*S4*). Since transformation media correspond to mere coordinate transformations of flat space, their geometry is Euclidean, with vanishing Riemann tensor,

$$R^i{}_{jkl} = 0 \ . \tag{S11}$$

In three-dimensional space the Riemann tensor vanishes if and only if the Ricci tensor is zero (*S6*),

$$R_{ij} = 0 \ . \tag{S12}$$

Conversely, if the effective Riemann or Ricci tensor of a dielectric material vanish, one can always find a coordinate transformation to flat space. Therefore the condition (S12) uniquely describes all possible spatial transformation media.

In flat Cartesian space, the natural solutions of Maxwell's equations are plane waves. If they are transformed by the medium they appear as modulated plane waves in physical space. To describe them, we simply express the Cartesian plane waves in a coordinate-independent form,

$$E_i = \mathcal{E}_i \, \mathrm{e}^{\mathrm{i}\varphi} , \quad \varphi = \int k_i \, \mathrm{d}x^i - \omega \, t \tag{S13}$$

with the dispersion relation

$$g^{ij} \, k_i \, k_j = \frac{\omega^2}{c^2} \ , \tag{S14}$$

the transversality

$$g^{ij} \, k_i \, \mathcal{E}_j = 0 \tag{S15}$$

and the continuity of the amplitude

$$\nabla^i \, \mathcal{E}_i = 0 \ . \tag{S16}$$

Equations (S13-S16) show that in transformation media geometrical optics is exact for incident plane waves. Here we consider non-Euclidean geometries where the Riemann tensor does not vanish. However, we assume that the effect of curvature is small on scales compatible with the wavelength, a condition we quantitatively describe as

$$|R| \ll \frac{\omega^2}{c^2} \tag{S17}$$

where R is the curvature scalar $R = g^{ij}\, R_{ij}$. In this case, we can locally ignore the effect of curvature in comparison with the optical oscillations and thus regard our material as a local transformation medium where geometrical optics would be exact. Consequently, in the regime (S17) geometrical optics, as described by the relations (S13-S16), is an excellent approximation.

Stereographic projection

For our specific case of non-Euclidean cloaking we use a powerful, visual tool of geometry: the stereographic projection, invented by Ptolemy, the basis of the Mercator projection in cartography (*S7*). The stereographic projection maps the surface of a sphere, a curved space, onto a plane. We denote the coordinates of points on the sphere by X, Y, Z and the Cartesian coordinates of the plane by x and y. The sphere with radius a is mapped onto the plane as shown in Fig. S1 according to the expressions

$$x = \frac{X}{1 - Z/a} \;, \quad y = \frac{Y}{1 - Z/a} \tag{S18}$$

with

$$X^2 + Y^2 + Z^2 = a^2 \;. \tag{S19}$$

Conversely, the plane is mapped onto the sphere as

$$X = \frac{2\,a\,x}{x^2 + y^2 + a^2} \;, \quad Y = \frac{2\,a\,y}{x^2 + y^2 + a^2} \;, \quad Z = a\,\frac{x^2 + y^2 - a^2}{x^2 + y^2 + a^2} \,. \tag{S20}$$

We obtain from the expressions (S20) the line element

$$\mathrm{d}X^2 + \mathrm{d}Y^2 + \mathrm{d}Z^2 = \frac{4\,a^4}{(x^2 + y^2 + a^2)^2}\; (\mathrm{d}x^2 + \mathrm{d}y^2) \;. \tag{S21}$$

The Riemann curvature of the sphere appears as a position-dependent factor in front of $\mathrm{d}x^2 + \mathrm{d}y^2$, which makes the stereographic coordinates particularly suitable for describing the geometry of a spherical surface. In contrast, in standard spherical coordinates with

$$X = a\,\cos\phi\,\sin\theta \,, \quad Y = a\,\sin\phi\,\sin\theta \,, \quad Z = a\,\cos\theta \tag{S22}$$

the line element is

$$\mathrm{d}X^2 + \mathrm{d}Y^2 + \mathrm{d}Z^2 = a^2(\mathrm{d}\theta^2 + \sin^2\theta\; \mathrm{d}\phi^2) \;. \tag{S23}$$

The stereographic coordinates are conformal: they assign a different measure of length, but the angles between lines on the sphere and their images on the plane are the same. An isotropic dielectric medium with refractive index n also changes the measure of space for light, but not the angles between light rays (*S1*). In two dimensions, it corresponds to the line element (*S1*)

$$\mathrm{d}s = n^2(\mathrm{d}x^2 + \mathrm{d}y^2) \;. \tag{S24}$$

One can thus implement the geometry of a sphere using the refractive index profile (*S1*)

$$n = \frac{2\,a^2}{x^2 + y^2 + a^2}\ . \tag{S25}$$

A device with the index profile (S25) is known as Maxwell's Fish Eye (*S8, S9*) and we will use it as one of the central building blocks of three-dimensional non-Euclidean cloaking devices. We also use another well-known property of the stereographic projection: circles on the sphere are mapped onto circles on the plane and vice versa. For example, on the sphere light propagates along the geodesics that are the great circles. The stereographic projections of these circles are circles as well. So, in Maxwell's Fish Eye light goes around in circles. On the sphere, the great circles originating from one point all meet at the antipodal point; so the light rays in the Fish Eye form perfect foci at two points, the original and the image. Maxwell's Fish Eye makes a perfect lens (*S10*).

Bipolar coordinates

Another convenient mathematical ingredient for our specific examples of cloaking devices are bipolar coordinates. By stereographic projection of the spherical coordinates (S22) we obtain a form of the polar coordinates

$$x = \cot(\theta/2)\,\cos\phi\ , \quad y = \cot(\theta/2)\,\sin\phi\ . \tag{S26}$$

On the other hand, if we tilt the sphere such that it lies on the side (like planet Uranus) we obtain the bipolar coordinates, see Fig. S2. We parametrize the surface of the sphere as

$$X = a\,\tanh\tau\ , \quad Y = a\,\operatorname{sech}\tau\,\sin\sigma\ , \quad Z = a\,\operatorname{sech}\tau\,\cos\sigma \tag{S27}$$

where the angle σ, the longitude, runs from $-\pi$ to π and the parameter τ from $-\infty$ to $+\infty$. One can easily verify that $X^2 + Y^2 + Z^2 = a^2$. By stereographic projection we obtain

$$x = \frac{a\,\sinh\tau}{\cosh\tau - \cos\sigma}\ , \quad y = \frac{a\,\sin\sigma}{\cosh\tau - \cos\sigma}\ . \tag{S28}$$

Note that the τ parametrization was chosen such that the x and y represent the real and the imaginary parts of an analytic function (*S7*)

$$x + \mathrm{i}\,y = \mathrm{i}\,a\,\cot\left(\frac{\sigma + \mathrm{i}\,\tau}{2}\right)\ , \tag{S29}$$

with the inverse function

$$\sigma + \mathrm{i}\,\tau = 2\,\mathrm{i}\,\operatorname{arcoth}\left(\frac{x + \mathrm{i}\,y}{a}\right)\ . \tag{S30}$$

Analytic functions describe conformal maps on the plane; so the bipolar coordinates are conformal, the Cartesian line element $\mathrm{d}x^2 + \mathrm{d}y^2$ deviates from $\mathrm{d}\sigma^2 + \mathrm{d}\tau^2$ by merely a prefactor. In particular we obtain

$$\mathrm{d}x^2 + \mathrm{d}y^2 = a^2 \, \frac{\mathrm{d}\sigma^2 + \mathrm{d}\tau^2}{(\cosh\tau - \cos\sigma)^2} \; . \tag{S31}$$

On the sphere the σ and τ coordinate lines form an orthogonal grid of circles. Therefore, as a consequence of the properties of the stereographic projection, the bipolar coordinate lines represent an orthogonal grid of circles as well. The circular coordinate lines are described by the equations

$$x^2 + (y - a\cot\sigma)^2 = \left(\frac{a}{\sin\sigma}\right)^2 , \tag{S32}$$

$$(x - a\coth\tau)^2 + y^2 = \left(\frac{a}{\sinh\tau}\right)^2 , \tag{S33}$$

as one easily verifies using Eq. (S28). Figure S2 shows the orthogonal grid of circles drawn by the bipolar coordinates.

Branches

We plan to incorporate the geometry of a plane and a sphere in the plane, as illustrated in Fig. 2A of our paper. We map the plane onto two branches that span the electromagnetic space of the cloaking device. One branch should represent the plane and the other the sphere. The branches are similar to the Riemann sheets of complex analysis (*S11*), apart from an important difference. The map we are going to use is not conformal and the dielectric functions that implement it do not tend to zero at the branch points, see Section *Implementation*. For defining the branches we use bipolar coordinates; we map σ of physical space to σ' of electromagnetic space where $\sigma'(\sigma)$ is an odd function for $-\pi \le \sigma \le \pi$. In electromagnetic space, σ' runs from -2π to 2π such that the primed coordinates cover the plane twice. It is reasonable to require that σ' agrees with σ outside of the device, for example outside a circle of radius a around the origin that, in bipolar coordinates, is described as $|\sigma| \le \pi/2$. Inside the device, for $|\sigma| > \pi/2$, σ' should be monotonically growing, faster than σ, such that σ' reaches $\pm 2\pi$ at $\sigma = \pm\pi$. It is wise to use a nonlinear function $\sigma'(\sigma)$ inside the device with smooth derivative at the boundary, because in this case the dielectric properties of the material are smooth such that the reflection of light at boundaries is avoided in practical implementations (*S3*). We thus require that $\mathrm{d}\sigma'/\mathrm{d}\sigma = 1$ at $\sigma = \pi/2$ and use a quadratic function for $\sigma'(\sigma)$ that reaches 2π at $\sigma = \pi$. We obtain

$$\sigma' = \begin{cases} \sigma & \text{for} \quad |\sigma| \le \dfrac{\pi}{2} \\ \operatorname{sgn}\sigma \left(\dfrac{4\sigma^2}{\pi} - 3|\sigma| + \pi \right) & \text{for} \quad \dfrac{\pi}{2} < |\sigma| \le \pi \end{cases} \tag{S34}$$

and therefore

$$\sigma = \begin{cases} \sigma' & \text{for} \quad |\sigma'| \leq \dfrac{\pi}{2} \\ \dfrac{\operatorname{sgn}\sigma'}{8}\left(3\pi + \sqrt{16\pi|\sigma'| - 7\pi^2}\right) & \text{for} \quad \dfrac{\pi}{2} < |\sigma'| \leq 2\pi \end{cases} . \tag{S35}$$

Figure S3 shows a plot of $\sigma(\sigma')$. One can use the complex representation (S29) of the bipolar coordinates to elegantly describe the transformation from the two branches of electromagnetic space to the physical plane in Cartesian coordinates. For the outer branch, containing the exterior of the device and the outer layer of the cloak, one should use

$$\sigma' + \mathrm{i}\,\tau = 2\,\mathrm{i}\,\operatorname{arcoth}\left(\frac{x' + \mathrm{i}\,y'}{a}\right) \tag{S36}$$

with the branch of arcoth shown in Fig. S4. Equation (S35) transforms σ' to the σ of physical space with the Cartesian coordinates (S29). In the next section we discuss the inner layer of the cloaking device, the non-Euclidean branch. There we use the branch of arcoth illustrated in Fig. S5 and map σ' and τ onto the surface of a sphere.

Non-Euclidean branch

We wish to map the inner branch of the device onto the surface $\{X', Y', Z'\}$ of a sphere with radius r_0, as Fig. 2A of our paper shows. For this, we identify σ' as the angle of longitude and conformally map the $\{X', Y', Z'\}$ sphere onto a $\{X, Y, Z\}$ sphere. Here the circles of equal latitude on $\{X', Y', Z'\}$ are compressed such that, on the $\{X, Y, Z\}$ sphere, they lie between a point on the equator and the south pole, see Fig. S6. Then we identify the deformed latitudinal lines with the τ lines of the bipolar coordinates. This procedure is best described in stereographic projection. We represent the spherical coordinates of the $\{X', Y', Z'\}$ sphere in terms of the dimensionless complex number z' as

$$X' + \mathrm{i}\,Y' = \frac{2\,r_0\,z'}{1 + |z'|^2} , \quad Z' = r_0\,\frac{|z'|^2 - 1}{|z'|^2 + 1} \tag{S37}$$

where, in spherical coordinates,

$$z' = \mathrm{e}^{\mathrm{i}\sigma'}\cot(\theta/2) . \tag{S38}$$

Here we have already identified the longitudinal angle with σ'. We also express the X, Y, Z sphere in terms of

$$X + \mathrm{i}\,Y = \frac{2\,r_0\,z}{1 + |z|^2} , \quad Z = r_0\,\frac{|z|^2 - 1}{|z|^2 + 1} . \tag{S39}$$

The Möbius transformation (*S7*)

$$z' = \frac{z}{1 + z} , \quad z = \frac{z'}{1 - z'} \tag{S40}$$

represents the desired transformation, because $z'(z)$ is analytic and hence conformal and $z'(z)$ maps the equatorial $z = -1$ onto the north pole at $z' = \infty$, and the south pole $z = 0$ onto the south pole $z' = 0$. Finally, we match θ and τ at the branch cut $\sigma' = \pm\pi$. First, consider the coordinates of the outer branch where in Eq. (S28) we replace x, y by x', y'. At the branch cut, $y' = 0$ and x' reaches

$$x'_0 = \frac{a \, \sinh \tau}{\cosh \tau + 1} \ . \tag{S41}$$

Now consider the inner, non-Euclidean branch. At the branch cut, where sphere and plane touch, the x'_0 line represents the angle on the sphere with

$$x'_0 = r_0 \, \arctan \frac{Z}{X} - a \ . \tag{S42}$$

Since the south pole $X = 0$ should correspond to the branch point $x'_0 = +a$ and the equatorial point $Z = 0$ to the other branch point $x'_0 = -a$, we get

$$r_0 = \frac{4}{\pi} \, a \ . \tag{S43}$$

Furthermore, at the branch cut $\sigma' = \pm\pi$ we obtain from Eqs. (S38-S40)

$$\frac{Z}{X} = \frac{2 + \tan(\theta/2)}{2 + 2 \cot(\theta/2)} \ . \tag{S44}$$

From this follows the connection between θ and τ. We easily derive explicit expressions for the Cartesian coordinates in the x, y plane, using the bipolar representation (S28) and writing $\cosh \tau$ and $\sinh \tau$ as functions of x'_0 deduced from Eq. (S41). We obtain

$$x = \frac{2 \, a^2 \, x'_0}{a^2 + {x'_0}^2 - (a^2 - {x'_0}^2) \cos \sigma} \ , \quad y = \frac{a \, (a^2 - {x'_0}^2) \sin \sigma}{a^2 + {x'_0}^2 - (a^2 - {x'_0}^2) \cos \sigma} \tag{S45}$$

with $\sigma(\sigma')$ given by Eq. (S35) and x'_0 by

$$x'_0 = \frac{4 \, a}{\pi} \, \arctan \left(\frac{2 + \tan(\theta/2)}{2 + 2 \cot(\theta/2)} \right) - a \ . \tag{S46}$$

To implement the non-Euclidean geometry of the sphere by a suitable material one should employ the effective electromagnetic geometry that corresponds to the line element

$$\mathrm{d}s^2 = \frac{16 \, a^2}{\pi^2} \, \left(\mathrm{d}\theta^2 + \sin^2 \theta \ \mathrm{d}{\sigma'}^2 \right) \ . \tag{S47}$$

Our matching procedure guarantees that the geometry of the non-Euclidean branch seamlessly fits the Euclidean geometry of the outer branch. In this way, one may implement the joint geometry of a sphere and a plane, the ingredients of a two-dimensional non-Euclidean cloaking device.

Holes and mirrors

But so far we have not constructed an invisibility device yet. The joint geometry of sphere and plane still covers the entire physical space where no place is hidden. However, we can easily exploit the non-Euclidean features of light propagation for creating invisible regions. They are visualized on the sphere of Fig. 2A of our paper (bearing in mind that this sphere and the light propagating on it has a faithful representation in physical space, see Fig. 2B). On the sphere, light rays propagate along geodesics, the great circles. Rays originating from one point fan out, focus on the antipodal point and then return to their origin. The entrance from the Euclidean part to the sphere, the branch cut, is a piece of geodesic as well, a quarter great circle. The rays originating from there will never cross the red zigzag indicated in Fig. 2A of our paper. This line is another quarter of the same great circle and touches the branch cut at a single point. Since light never crosses this line we can inflate the line, expanding it in the same way as we have expanded the physical plane to accommodate the surface of the sphere. Now the interior of the expanded line is a hidden space, inaccessible to light. Another option requires the use of a mirror. Imagine a mirror around the equator of the sphere, see Fig. 2C of our paper. The reflected light rays faithfully return to their origin, but the top of the sphere is hidden behind the mirror. In physical space, light rays would follow trajectories like the one shown in Fig. S7.

Let us put the first option into analytical geometry. The red line on the sphere corresponds, on the physical plane, to the line between $(-a, 0)$ and $(x_a, 0)$ with

$$x'_a = x'_0\Big|_{\theta=\pi/2} = \frac{4\,a}{\pi}\,\arctan\left(\frac{3}{4}\right) - a\ . \tag{S48}$$

We may adapt our previous procedure for opening up a line, the branch cut between $-a$ and $+a$, using the conformal linear transformation

$$\Big(x, y\Big) \to \frac{a}{a + x_a}\Big(a - x_a + 2x, 2y\Big) \tag{S49}$$

followed by the expansion described in Section *Branches* and the inverse transformation

$$\Big(x, y\Big) \to \frac{a + x_a}{2a}\left(x - a\,\frac{a - x_a}{a + x_a}, y\right)\ . \tag{S50}$$

Let us describe the second option, the mirror, in terms of stereographic coordinates (S37) where the reflection at the mirror around the equator of the sphere corresponds to the reflection at a circle. If z' describes, in stereographic coordinates, the position of a light ray on the sphere, the reflected light is

$$z' \to \frac{1}{z'^*} \quad \text{for} \quad |z'| > 1\,. \tag{S51}$$

Using this mirror transformation we obtain the trajectory illustrated in Fig. S7. Note that in physical space the rays do not obey the law that the angle of reflection equals the angle of incidence. This seems strange at first sight, but if the mirror is enclosed by an anisotropic material, which is the case here, then this law does not hold anymore.

Three-dimensional case

In this section we explain how our ideas can be extended to cloaking in three-dimensional space. First, we introduce three-dimensional branches where the x, y, z coordinates of physical space[1] cover the x', y', z' coordinates of electromagnetic space twice. This is easily done by rotating our two-dimensional branches around the y axis. The bipolar coordinates turn into toroidal coordinates,

$$\begin{aligned} x &= \frac{a\,\sinh\tau\cos\chi}{\cosh\tau-\cos\sigma} \quad , \quad y = \frac{a\,\sin\sigma}{\cosh\tau-\cos\sigma} \quad , \quad z = \frac{a\,\sinh\tau\sin\chi}{\cosh\tau-\cos\sigma}\,, \\ x' &= \frac{a\,\sinh\tau\cos\chi}{\cosh\tau-\cos\sigma'} \quad , \quad y' = \frac{a\,\sin\sigma'}{\cosh\tau-\cos\sigma'} \quad , \quad z' = \frac{a\,\sinh\tau\sin\chi}{\cosh\tau-\cos\sigma'}\,, \end{aligned} \tag{S52}$$

where we use the same σ transformation (S35) as in the two-dimensional case. The outer branch is Euclidean and includes the exterior of the device ($|\sigma'| < \pi/2$), while the inner branch is non-Euclidean. In three dimensions, the branch cut is a two-dimensional surface. Here the Euclidean geometry of the outer branch should smoothly evolve into the non-Euclidean geometry at the core of the device, in order to avoid refraction and reflection at the boundary (*S3*). To give a specific example, we employ the three-dimensional surface of a four-dimensional hypersphere as non-Euclidean space. The surface of the hypersphere is conveniently described in three-dimensional generalizations x', y', z' of the stereographic coordinates with the metric

$$\mathrm{d}s^2 = n'^2\left(\mathrm{d}x'^2 + \mathrm{d}y'^2 + \mathrm{d}z'^2\right) \tag{S53}$$

where we made a slight modification of the Fish-Eye profile (S25)

$$n' = \frac{4\,a^2}{2\,a^2 + x'^2 + (y'-a)^2 + z'^2}\,. \tag{S54}$$

The n' corresponds to the refractive-index profile of the inner branch of electromagnetic space. Just as in the two-dimensional case, Maxwell's Fish Eye represents the geometry of a sphere, in three dimensions it represents the geometry of the three-dimensional surface of a four-dimensional hypersphere. We have moved the center of the hypersphere to the point $(0, a, 0)$. At the distance $\sqrt{2}\,a$ from the center the refractive index n' is unity; this is where the equator of the hypersphere touches the x', y', z' space in the four-dimensional case of the stereographic projection, the four-dimensional equivalent of Fig. S1. (In four dimensions the equator of the hypersphere is a two-dimensional surface — a sphere — and the stereographic projection plane has become the three-dimensional space x', y', z'.) So the radius of the hypersphere is $\sqrt{2}\,a$. In the non-Euclidean branch, the ray trajectories, the geodesics, correspond to the great circles on the hypersphere. In stereographic projection, they are circles in x', y', z' space that intersect the

[1] From here on z denotes one of the Cartesian coordinates.

equatorial sphere at two antipodal points. If we chose as branch cut a segment of the equatorial sphere, light entering there performs complete loops before leaving through the branch cut, provided the segment is sufficiently small. It should be smaller than a hemisphere such that the antipodal points are excluded where light could leave through the branch cut without completing a loop in electromagnetic space. We choose the spherical cap shown in Fig. S8. In terms of the toroidal coordinates (S52) our branch cut corresponds to $\sigma' = -3\pi/4$ in one branch of electromagnetic space. Adding 2π we obtain $\sigma' = 5\pi/4$ in the other branch. In physical space, the two corresponding σ values describe the two sides of the branch cut, two spherical caps, one with $\sigma = -(3+\sqrt{5})\pi/8$ and the other with $\sigma = (3+\sqrt{13})\pi/8$, as we see from Eq. (S35). These spherical caps enclose the inner layer of the cloaking device.

Note that some rays in the Euclidean branch of electromagnetic space, following straight lines there, may pierce the curved branch cut twice, as Fig. S8 also shows. Such rays would perform two loops in the non-Euclidean branch. In contrast, in our two-dimensional case rays perform single loops if any. We are sceptical whether such simple-loop branch cuts exist on the three-dimensional surface of the four-dimensional hypersphere; so our example is probably generic.

In Cartesian coordinates, the transformation from the two branches of electromagnetic space to physical space is described as follows: for the outer branch one should use

$$\sigma' + \mathrm{i}\,\tau = 2\,\mathrm{i}\,\mathrm{arcoth}\left(\frac{\sqrt{x'^2+z'^2}+\mathrm{i}\,y'}{a}\right) \tag{S55}$$

with the branch of arcoth shown in Fig. S9 and for the non-Euclidean part of the device the branch of Fig. S10. We add or substract 4π from σ' such that σ' lies between -2π and 2π, and calculate σ according to Eq. (S35). We obtain in Cartesian coordinates

$$\begin{aligned} x &= -\frac{a\,x'}{\sqrt{x'^2+z'^2}}\,\mathrm{Im}\left(\cot\frac{\sigma+\mathrm{i}\,\tau}{2}\right), \\ y &= a\,\mathrm{Re}\left(\cot\frac{\sigma+\mathrm{i}\,\tau}{2}\right), \\ z &= -\frac{a\,z'}{\sqrt{x'^2+z'^2}}\,\mathrm{Im}\left(\cot\frac{\sigma+\mathrm{i}\,\tau}{2}\right). \end{aligned} \tag{S56}$$

In order to turn our non-Euclidean transformation medium into a cloaking device, we may follow similar strategies as in the two-dimensional case: we expand an area that light never enters or hide a region behind a mirror. For example, light does not cross the spherical cap shown in Fig. S11. We may regard this two-dimensional surface as another branch cut, as the two sides of a flattened volume that we inflate like a balloon using a similar procedure as before. We move our toroidal coordinate system to the boundary of the hidden area, planting its poles at $(-a,0,0)$ and $(-a,2a,0)$. Figure S12 shows a diagram of the branch cuts described in the moved coordinates σ'_1 and τ'_1. Light enters through an arc segment at $\sigma'_1 = \pi/4$. The second

branch cut, the one we wish to expand to a hidden space, corresponds to $\sigma_1' = -3\pi/4$ or, equivalently, $\sigma_1' = 5\pi/4$. We describe our expansion procedure in Cartesian coordinates as

$$\begin{aligned} x' &= -a + a\,\mathrm{Re}\left(\cot\frac{\sigma_1' + \mathrm{i}\,\tau_1'}{2}\right), \\ y' &= a - \frac{a\,(y''-a)}{\sqrt{(y''-a)^2 + z''^2}}\,\mathrm{Im}\left(\cot\frac{\sigma_1' + \mathrm{i}\,\tau_1'}{2}\right), \\ z' &= -\frac{a\,z''}{\sqrt{(y''-a)^2 + z''^2}}\,\mathrm{Im}\left(\cot\frac{\sigma_1' + \mathrm{i}\,\tau_1'}{2}\right). \end{aligned} \tag{S57}$$

where σ_1' is a suitable function of σ_1'' with

$$\sigma_1'' + \mathrm{i}\,\tau_1' = 2\,\mathrm{i}\,\mathrm{arcoth}\left(\frac{\sqrt{(y''-a)^2 + z''^2} + \mathrm{i}\,x'' + \mathrm{i}\,a}{a}\right) \tag{S58}$$

and the branch of arcoth chosen according to Fig. S9. It remains to specify σ_1''. What are the requirements? At the entrance of the non-Euclidean branch, $\sigma_1' = \pi/4$, the outer layer of the cloaking device should smoothly fit the inner layer. Hence we require for $\sigma_1'' = \pi/4$ that $\sigma_1'(\sigma_1'') = \pi/4$ and $\mathrm{d}\sigma_1'/\mathrm{d}\sigma_1'' = 1$. In order to create a hidden space, we may deform one side of the second branch cut into the line segment at $\sigma_1'' = 0$ and the other side into $\sigma_1'' = \pi$, as shown in Fig. S12. In this way, the entire left side of electromagnetic space, for $y' < -a$, is hidden. We thus require that $\sigma_1'(-3\pi/4) = 0$ and $\sigma_1'(5\pi/4) = \pi$. We fit the inverse function $\sigma_1''(\sigma_1')$ by two quadratic functions, one for $0 \le \sigma_1' \le \pi/4$ and the other for the interval $\pi/4 \le \sigma_1' \le \pi$ according to our requirements. We obtain for $\sigma_1'(\sigma_1'')$ the expressions

$$\sigma_1' = \begin{cases} \frac{1}{24}\left(7\pi - \sqrt{13\pi^2 - 48\pi\,\sigma_1''}\right) & \text{for} \quad -\dfrac{3\pi}{4} \le \sigma_1'' \le \dfrac{\pi}{4} \\ \frac{1}{8}\left(-7\pi + 3\sqrt{5\pi^2 + 16\pi\,\sigma_1''}\right) & \text{for} \quad \dfrac{\pi}{4} \le \sigma_1'' \le \dfrac{5\pi}{4} \end{cases}. \tag{S59}$$

Equations (S55-S59) describe the branches of the cloaking device. The outer branch of electromagnetic space $\{x', y', z'\}$ is empty, the refractive index is unity. In the inner branch of $\{x', y', z'\}$ space we performed a second expansion and use the geometry of a hypersphere implemented by the Fish-Eye profile (S54) in $\{x'', y'', z''\}$ space,

$$n'' = \frac{4\,a^2}{2\,a^2 + x''^2 + (y''-a)^2 + z''^2}. \tag{S60}$$

Figures 3A and 3B of our paper show ray trajectories for this situation. We obtain the trajectories by solving Hamilton's equations for the rays in each branch and transforming the trajectories to physical space according to Eqs. (S55-S59).

Let us turn to our other option for creating a hidden space, the mirror. Imagine we place a tilted plane mirror in electromagnetic x', y', z' space behind the branch cut, see Fig. S13.

The trajectory of the reflected light forms the mirror image of the trajectory behind the plane covered by the mirror. Like in the two-dimensional case illustrated in Fig. 2C of our paper, the light should return to the entrance of the non-Euclidean branch as if the mirror (and everything hidden behind it) would not be there. To see this, consider the following. The part of the ray trajectory that is to be reflected lies on the "southern hemisphere" of the hypersphere, because the incident part of the trajectory has crossed the equator and so lies partially on the "northern hemisphere" of the hypersphere. The reflected light will remain on the "southern hemisphere" and so will not leave through the branch cut too early, but complete the loop. The space behind the mirror remains invisible and its presence undetectable. To turn these ideas into analytical geometry, we note that in electromagnetic space the plane of the mirror is located at

$$y' = x' + a\,. \tag{S61}$$

To determine the mirror image of ray trajectories, we shift the Cartesian coordinates x', y', z' by $-a$ in y direction, rotate the coordinate system by $\pi/4$ such that it aligns with the mirror, reverse the component of the ray's position vector that is orthogonal to the mirror, and finally move the coordinate frame back to the original position. The result is the transformation

$$\Big(x', y', z'\Big) \to \Big(y' - a\,,\, x' + a\,,\, z'\Big) \quad \text{for} \quad y' > x' + a\ . \tag{S62}$$

Figure S14 shows an example of the corresponding ray trajectories. We traced the trajectories by solving Hamilton's equations in electromagnetic space with the Fish-Eye profile (S54) in the inner, non-Euclidean branch, performing there the mirror transformation (S62) for $y' > x' + a$, and then transforming the ray to physical space.

Implementation

In this section we calculate the material properties required to implement our device. We focus on the simplest case for implementation, the three-dimensional cloaking device with mirrors. Our other specific examples will not differ much from this case. Note however that one could construct invisibility devices of arbitrary shapes by further coordinate transformations of our examples within the same topology. This would of course alter the required material properties. One can imagine finding the optimal parameters by deforming the profile of the cloaking device within the constraints of a particular application. The purpose of the calculation here is simply to give an example without attempting to optimize the practical requirements.

It is convenient to perform this calculation in toroidal coordinates. First, we write down the line element of the geometry we wish to implement and then we follow the recipe outlined in Section *Geometry and media*. In electromagnetic space, the inner branch of the cloaking device carries the Fish-Eye profile (S54), whereas the outer branch is empty space. The branch cut at $\sigma' = -3\pi/4$ and $\sigma' = 5\pi/4$ corresponds to the values

$$\sigma_1 = -\frac{3\pi + \sqrt{5}\,\pi}{8}\,, \quad \sigma_2 = \frac{3\pi + \sqrt{13}\,\pi}{8} \tag{S63}$$

in physical space for our transformation (S35). The geometry is characterized by the line element

$$\mathrm{d}s^2 = n_{EM}'^2\ a^2\ \frac{\mathrm{d}\sigma'^2 + \mathrm{d}\tau^2 + \sinh^2\tau\,\mathrm{d}\chi^2}{(\cosh\tau - \cos\sigma')^2} \tag{S64}$$

where n'_{EM} denotes the index profile in electromagnetic space expressed in toroidal coordinates,

$$n'_{EM} = \begin{cases} 1 & \text{for} \quad \sigma_1 \le \sigma \le \sigma_2 \\ \\ \dfrac{2\,(\cosh\tau - \cos\sigma')}{2\cosh\tau - \cos\sigma' - \sin\sigma'} & \text{otherwise} \end{cases} . \tag{S65}$$

From the line element we read off the metric tensor in physical space,

$$g_{ij} = \frac{n_{EM}'^2\,a^2}{(\cosh\tau - \cos\sigma')^2}\,\mathrm{diag}\left(\left(\frac{\mathrm{d}\sigma'}{\mathrm{d}\sigma}\right)^2,\ 1\,,\ \sinh^2\tau\right) . \tag{S66}$$

We calculate the determinant g and the inverse matrix g^{ij}, and obtain

$$g = \frac{n_{EM}'^6\,a^6\,\sinh^2\tau}{(\cosh\tau - \cos\sigma')^6}\left(\frac{\mathrm{d}\sigma'}{\mathrm{d}\sigma}\right)^2 , \tag{S67}$$

$$g^{ij} = \frac{(\cosh\tau - \cos\sigma')^2}{n_{EM}'^2\,a^2}\,\mathrm{diag}\left(\left(\frac{\mathrm{d}\sigma}{\mathrm{d}\sigma'}\right)^2,\ 1\,,\ \frac{1}{\sinh^2\tau}\right) . \tag{S68}$$

Then we calculate the mixed tensor $\varepsilon^i{}_j$ of the electric permittivity according to Eqs. (S4) and (S5). In the ideal case, the device is impedance-matched to the vacuum, so the magnetic permeability equals the electric permittivity. Equation (S4) depends on the background geometry, which is in our case the geometry of toroidal coordinates with metric tensor

$$\gamma_{ij} = \frac{a^2}{(\cosh\tau - \cos\sigma)^2}\,\mathrm{diag}\left(1\,,\ 1\,,\ \sinh^2\tau\right) \tag{S69}$$

and determinant

$$\gamma = \frac{a^6\,\sinh^2\tau}{(\cosh\tau - \cos\sigma)^6} . \tag{S70}$$

Consequently, we obtain for the electric-permittivity tensor in toroidal coordinates

$$\begin{aligned} \varepsilon^i{}_j &= n'_{EM}\,\frac{\cosh\tau - \cos\sigma}{\cosh\tau - \cos\sigma'}\,\mathrm{diag}\left(\frac{\mathrm{d}\sigma}{\mathrm{d}\sigma'}\,,\ \frac{\mathrm{d}\sigma'}{\mathrm{d}\sigma}\,,\ \frac{\mathrm{d}\sigma'}{\mathrm{d}\sigma}\right) , \\ &= n_0\,\mathrm{diag}\left(\frac{\mathrm{d}\sigma}{\mathrm{d}\sigma'}\,,\ \frac{\mathrm{d}\sigma'}{\mathrm{d}\sigma}\,,\ \frac{\mathrm{d}\sigma'}{\mathrm{d}\sigma}\right) \end{aligned} \tag{S71}$$

with

$$n_0 = \begin{cases} \dfrac{\cosh\tau - \cos\sigma}{\cosh\tau - \cos\sigma'} & \text{for} \quad \sigma_1 \le \sigma \le \sigma_2 \\ \\ \dfrac{2\,(\cosh\tau - \cos\sigma)}{2\cosh\tau - \cos\sigma' - \sin\sigma'} & \text{otherwise} \end{cases} . \tag{S72}$$

It is straightforward to express our result (S72) in Cartesian coordinates. We only have to determine the basis vectors (*S1*) for the toroidal coordinates (S52), because they form the eigenvectors of the dielectric tensor. The basis vectors are the derivatives of the Cartesian vector $\mathbf{r} = (x, y, z)$ with respect to the toroidal coordinates (*S1*),

$$\begin{aligned} \mathbf{e}_\sigma &= \frac{\partial \mathbf{r}}{\partial \sigma} = a \left(-\frac{\sin\sigma\, \sinh\tau\, \cos\chi}{(\cosh\tau - \cos\sigma)^2}, \frac{\cosh\tau\, \cos\sigma - 1}{(\cosh\tau - \cos\sigma)^2}, -\frac{\sin\sigma\, \sinh\tau\, \sin\chi}{(\cosh\tau - \cos\sigma)^2} \right), \\ \mathbf{e}_\tau &= \frac{\partial \mathbf{r}}{\partial \tau} = -a \left(\frac{(\cosh\tau\, \cos\sigma - 1)\cos\chi}{(\cosh\tau - \cos\sigma)^2}, \frac{\sinh\tau\, \sin\sigma}{(\cosh\tau - \cos\sigma)^2}, \frac{(\cosh\tau\, \cos\sigma - 1)\sin\chi}{(\cosh\tau - \cos\sigma)^2} \right), \\ \mathbf{e}_\chi &= \frac{\partial \mathbf{r}}{\partial \chi} = a \left(-\frac{\sinh\tau \sin\chi}{\cosh\tau - \cos\sigma}, 0, \frac{\sinh\tau \cos\chi}{\cosh\tau - \cos\sigma} \right) . \end{aligned} \tag{S73}$$

The basis vectors are orthogonal, because the toroidal coordinates form an orthogonal system. Of course, the eigenvectors of the dielectric tensor must be orthogonal, because $\varepsilon^i{}_j$ is a real and symmetric matrix. However, the $\mathbf{e}_\sigma, \mathbf{e}_\tau, \mathbf{e}_\chi$ are not normalized with respect to the Cartesian metric. We normalize them,

$$\begin{aligned} \hat{\mathbf{e}}_\sigma &= \left(-\frac{\sin\sigma\, \sinh\tau\, \cos\chi}{\cosh\tau - \cos\sigma}, \frac{\cosh\tau\, \cos\sigma - 1}{\cosh\tau - \cos\sigma}, -\frac{\sin\sigma\, \sinh\tau\, \sin\chi}{\cosh\tau - \cos\sigma} \right), \\ \hat{\mathbf{e}}_\tau &= \left(\frac{(\cosh\tau\, \cos\sigma - 1)\cos\chi}{\cosh\tau - \cos\sigma}, \frac{\sinh\tau\, \sin\sigma}{\cosh\tau - \cos\sigma}, \frac{(\cosh\tau\, \cos\sigma - 1)\sin\chi}{\cosh\tau - \cos\sigma} \right), \\ \hat{\mathbf{e}}_\chi &= (-\sin\chi,\, 0,\, \cos\chi) . \end{aligned} \tag{S74}$$

and arrive at the dielectric tensor ε_c in Cartesian coordinates

$$\varepsilon_c = n_0 \left[\frac{\mathrm{d}\sigma}{\mathrm{d}\sigma'}\, \hat{\mathbf{e}}_\sigma \otimes \hat{\mathbf{e}}_\sigma + \frac{\mathrm{d}\sigma'}{\mathrm{d}\sigma}\, (\hat{\mathbf{e}}_\tau \otimes \hat{\mathbf{e}}_\tau + \hat{\mathbf{e}}_\chi \otimes \hat{\mathbf{e}}_\chi) \right] \tag{S75}$$

with n_0 given by Eq. (S72) and using the function (S34) for $\sigma'(\sigma)$. It remains to express the toroidal coordinates σ, τ and χ in terms of the Cartesian x, y and z. One should be careful about choosing the correct branch for σ,

$$\sigma = \begin{cases} \arctan\left(\dfrac{2\,a\,y}{x^2 + y^2 + z^2 - a^2} \right) & \text{for} \quad x^2 + y^2 + z^2 \ge a^2 \\ \\ \arctan\left(\dfrac{2\,a\,y}{x^2 + y^2 + z^2 - a^2} \right) + \pi\,\mathrm{sgn}\, y & \text{otherwise} \end{cases} \tag{S76}$$

written in terms of the main branch of $\arctan$ that runs from $-\pi/2$ to $\pi/2$. The other toroidal coordinates are simply given by

$$\tau = \operatorname{artanh}\left(\frac{2\,a\,\sqrt{x^2+z^2}}{x^2+y^2+z^2+a^2}\right), \quad \cos\chi = \frac{x}{\sqrt{x^2+z^2}}, \quad \sin\chi = \frac{z}{\sqrt{x^2+z^2}} \tag{S77}$$

using the non-negative branch of the square root. In order to obtain the position of the mirror in physical space, one should translate the mirror equation (S61) from the second branch of electromagnetic space into the Cartesian coordinates of physical space. For this, one determines first σ', τ, and χ following the same procedure as in Eqs. (S76) and (S77), apart from adding $2\pi\,\operatorname{sgn} y'$ to σ' (in the second branch of electromagnetic space). One obtains σ from Eq. (S35) and finally translates the toroidal coordinates back to Cartesian coordinates according to their definition (S52).

What is the range of the dielectric functions required for implementing the device? Let us return to toroidal coordinates, because there the permittivity tensor is diagonal. The extrema of n_0 lie on the curve with $\tau = 0$, as differentiating n_0 with respect to τ proves. Figure S15a shows the curve of $n_0\,\mathrm{d}\sigma/\mathrm{d}\sigma'$ where ε reaches a minimum and Fig. S15b the curve of $n_0\,\mathrm{d}\sigma'/\mathrm{d}\sigma$ where ε is maximal. We numerically found the minimum value 0.28 and the maximum 31.2. We clearly see that the permittivity is finite and different from zero. This is not a coincidence, but a generic feature of our scheme that is preserved under further transformations to give cloaking devices any desired shape: neither the coordinate transformations nor the non-Euclidean geometry we employ are singular. The device alters the measure of space the electromagnetic field perceives, but these changes are gradual and finite. Even at the boundaries of branch cuts the measure of space does not shrink to zero, because we do not apply conformal transformations. We see from Eq. (S3) why finite distortions of the measure of space correspond to finite values of the dielectric properties. We obtain for the determinant $\det\varepsilon$ of $\varepsilon^i{}_j$ the expression

$$\det\varepsilon = \sqrt{\frac{g}{\gamma}}\,. \tag{S78}$$

The ratio $\sqrt{g/\gamma}$ describes the modification of the volume element (*S1*) and the determinant is the product of the eigenvalues. Consequently, the material properties required for non-Euclidean cloaking devices lie within a range that is, in principle, achievable for a broad band of the electromagnetic spectrum. Broadband invisibility seems feasible using ideas of non-Euclidean geometry.

References and Notes

S1. U. Leonhardt, T. G. Philbin, *Prog. Opt.* (in press); preprint arxiv:0805.4778.

S2. D. Schurig et al., *Science* **314**, 977 (2006).

S3. W. S. Cai, U. K. Chettiar, A. V. Kildishev, V. M. Shalaev, G. W. Milton, *Appl. Phys. Lett.* **91**, 111105 (2007).

S4. U. Leonhardt, T. G. Philbin, *New J. Phys.* **8**, 247 (2006).

S5. J. B. Pendry, D. Schurig, D. R. Smith, *Science* **312**, 1780 (2006).

S6. L. D. Landau, E. M. Lifshitz, *The Classical Theory of Fields* (Butterworth-Heinemann, Oxford, 1995).

S7. T. Needham, *Visual Complex Analysis* (Clarendon Press, Oxford, 2002).

S8. J. C. Maxwell, *Cambridge and Dublin Math. J.* **8**, 188 (1854).

S9. R. K. Luneburg, *Mathematical Theory of Optics* (University of California Press, Berkeley and Los Angeles, 1964).

S10. M. Born, E. Wolf, *Principles of Optics* (Cambridge University Press, Cambridge, 1999)

S11. M. J. Ablowitz, A. S. Fokas, *Complex Variables* (Cambridge University Press, Cambridge, 1997).

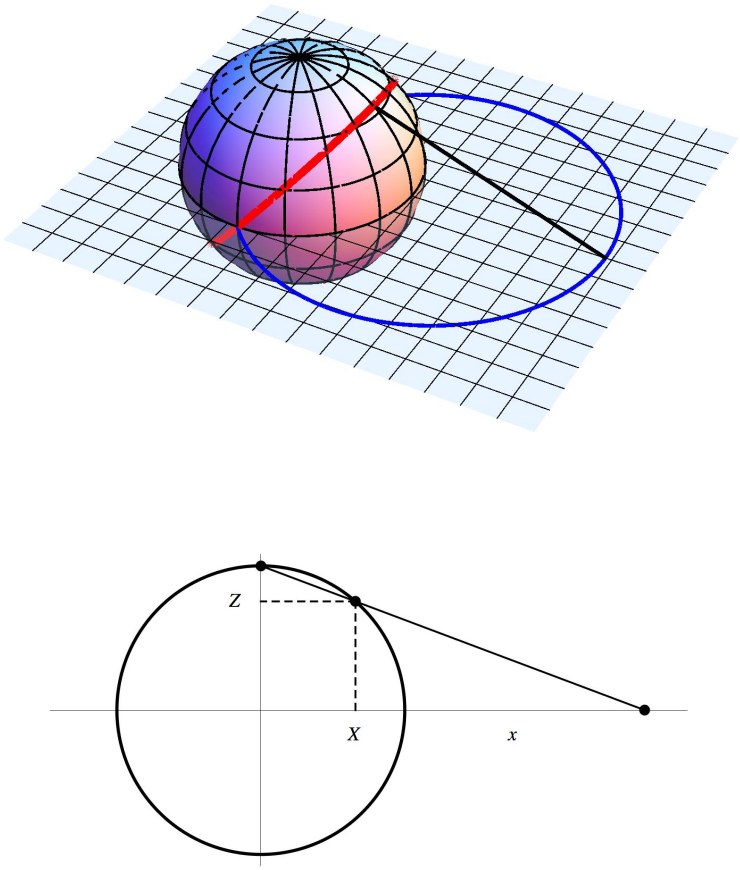

Figure S1: Stereographic projection. The surface of a sphere is mapped onto a plane cutting through the equator. The mapping is performed as follows: through each point on the surface of the sphere a line is drawn from the north pole. The image is the point where the line intersects the equatorial plane. Top: three-dimensional plot, showing that the image of a circle on the sphere is a circle on the plane. Bottom: two-dimensional diagram of the stereographic projection.

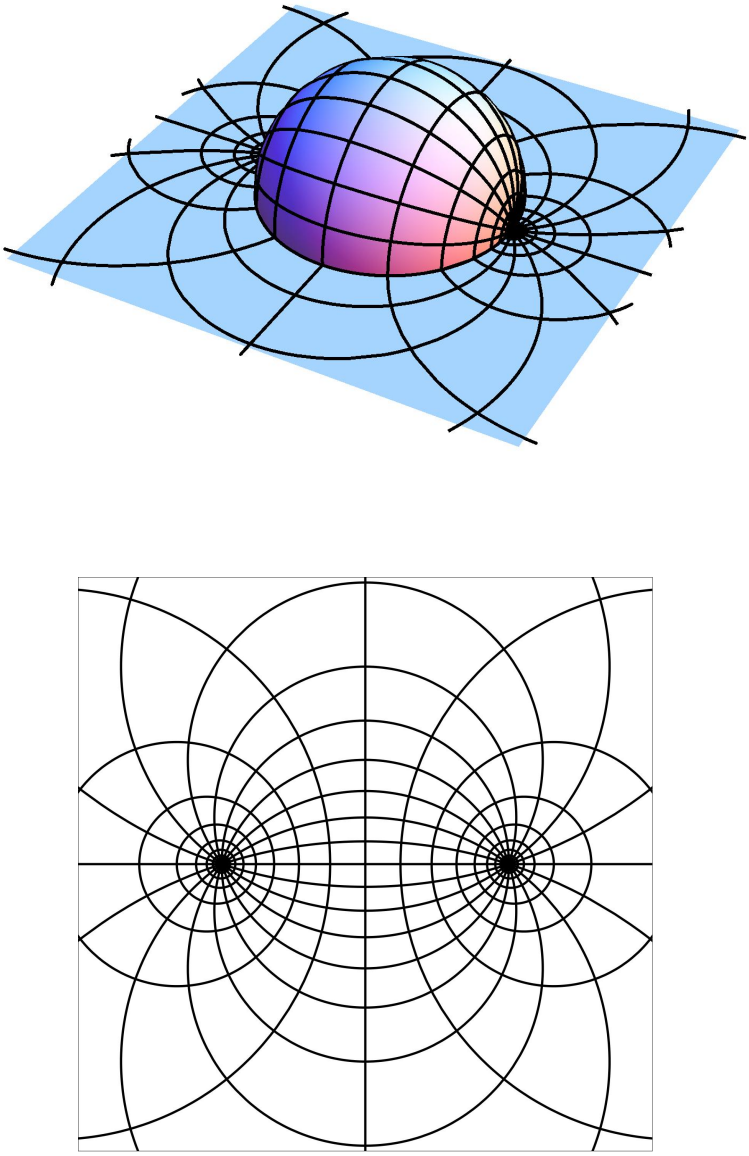

Figure S2: Bipolar coordinates via stereographic projection. Top: the coordinate grid of a sphere laying on the side is projected onto the equatorial plane. One obtains the bipolar coordinates shown below. The two poles of the sphere have become the two poles of the bipolar coordinates. Since the stereographic projection is a conformal map the coordinate lines are orthogonal to each other; since circles are mapped onto circles the bipolar coordinates form an orthogonal grid of circles.

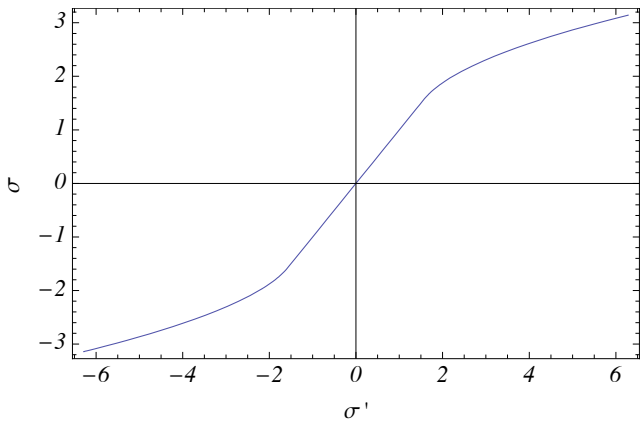

Figure S3: Transformation of bipolar angle. The figure shows a plot of the bipolar angle in physical space σ as a function of the bipolar angle in electromagnetic space σ'. In the interval $[-\pi/2, \pi/2]$ the bipolar angle is not changed; this interval correspond to the exterior of the cloaking device where the coordinates are not modified. The inverse transformation $\sigma'(\sigma)$ covers the range of the bipolar angle twice, creating two branches. The outer branch corresponds to $\sigma' \in [-\pi, \pi]$ and the inner branch to $[-2\pi, -\pi]$ combined with the interval $[\pi, 2\pi]$. The inner branch contains the non-Euclidean geometry of the cloaking device. The function $\sigma(\sigma')$ and its first derivative are smooth, even at the boundary of the device at $\sigma' = \pm\pi/2$. In this case, the dielectric functions that implement this geometry are smooth, for avoiding the reflection of light at sharp interfaces.

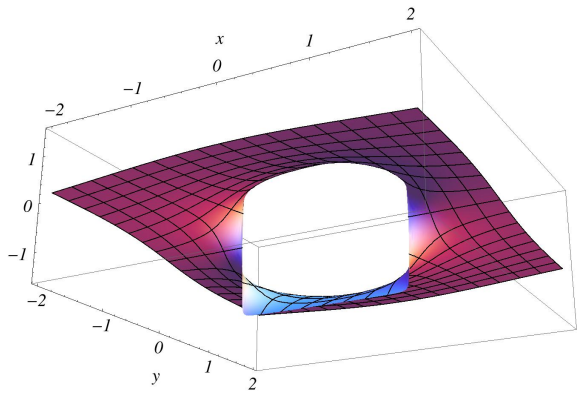

Figure S4: Branch of arcoth on the complex plane. The figure shows the imaginary part of $\mathrm{arcoth} z$ as a function of $z = x + \mathrm{i}y$.

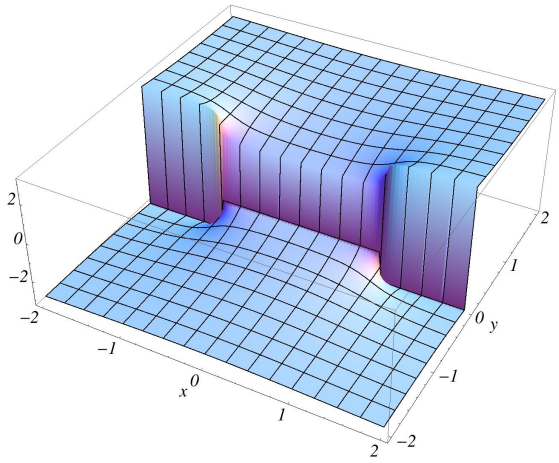

Figure S5: A second branch of arcoth on the complex plane. Description as in Fig. S4.

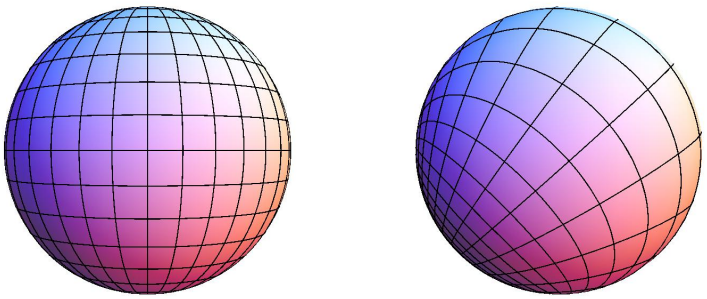

Figure S6: Conformal transformation on a sphere. The Möbius transformation (S40) in stereographic coordinates deforms the coordinate grid on the sphere (left to right). The grid remains orthogonal, because the transformation is conformal, but the north pole is moved to the equator while the south pole remains at the same place.

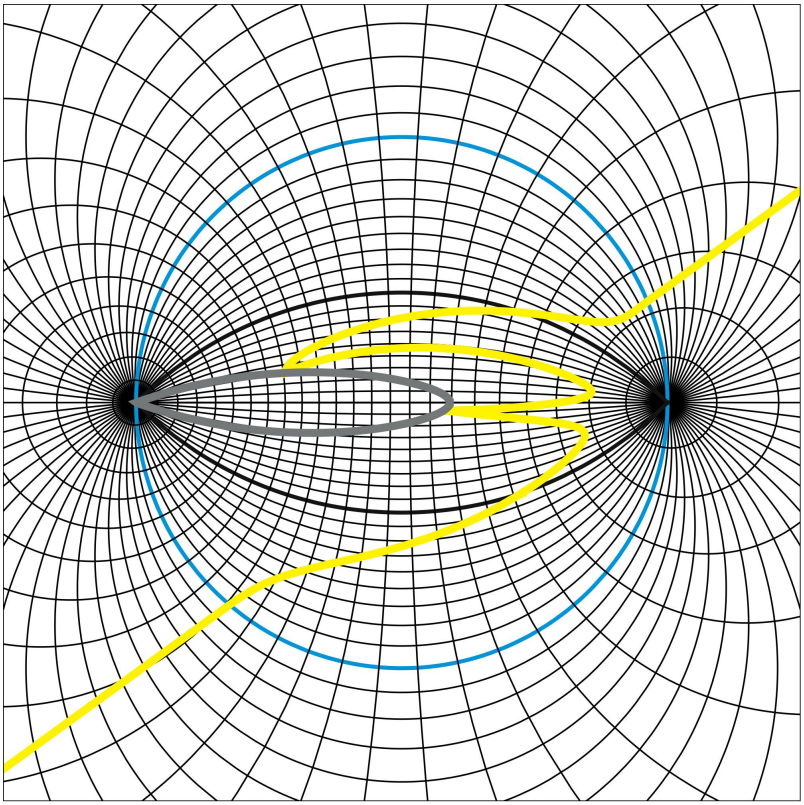

Figure S7: Hiding behind a mirror. Light entering the non-Euclidean branch of the cloaking device bounces off a mirror that encloses the invisible region. The mirror corresponds to the one shown in Fig. 2C of our paper that goes around the equator of the sphere in electromagnetic space. Description of the coordinate lines as in Fig. 2B.

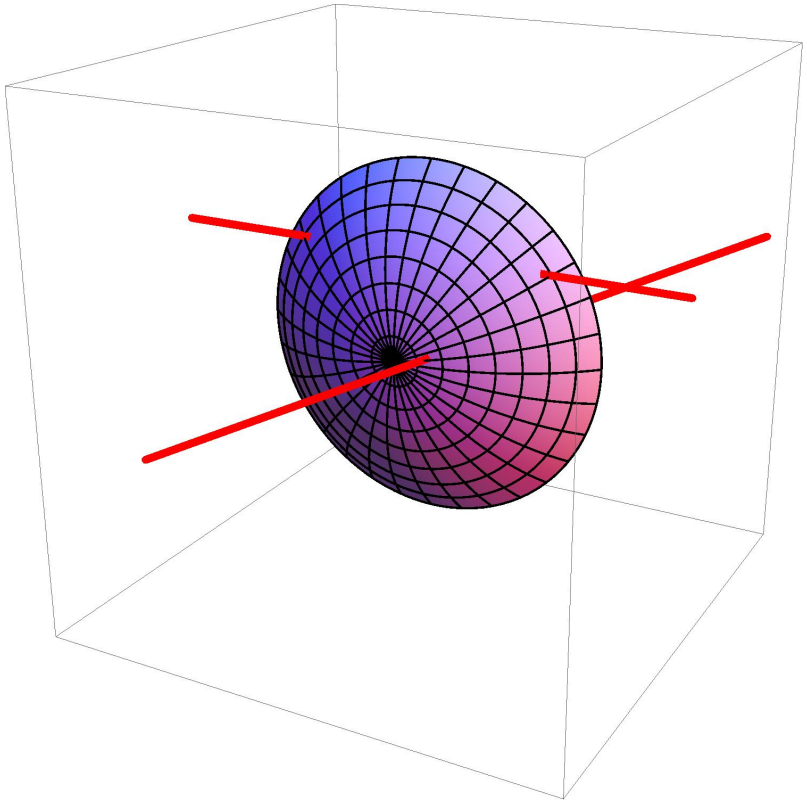

Figure S8: Branch cut in three dimensions. In three-dimensional electromagnetic space, the branch cut is a curved two-dimensional surface arranged such that the Euclidean geometry of the outer branch smoothly evolves into the non-Eucliean geometry of the inner branch. To achieve this, the branch cut is chosen to be the surface where the Fish-Eye profile (S54) agrees with the refractive index of empty space, unity. The figure also shows some light rays in red. Most rays intersect the branch cut only one time, but some pierce it twice. Such rays enter the non-Euclidean branch, perform a loop (not shown), return to the Euclidean branch, enter the branch cut a second time before they leave after another loop (not shown).

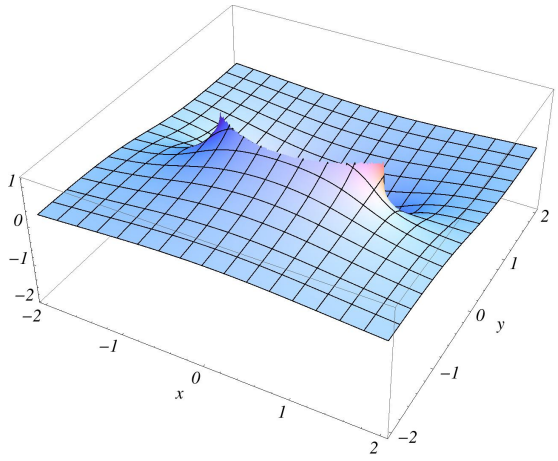

Figure S9: Branch of arcoth on the complex plane as required for three-dimensional cloaking where the branch cut is curved. Description as in Fig. S4.

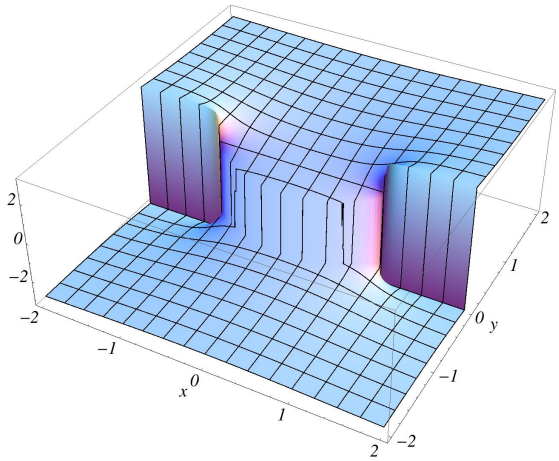

Figure S10: A second branch of arcoth on the complex plane as required for three-dimensional cloaking. Description as in Fig. S4.

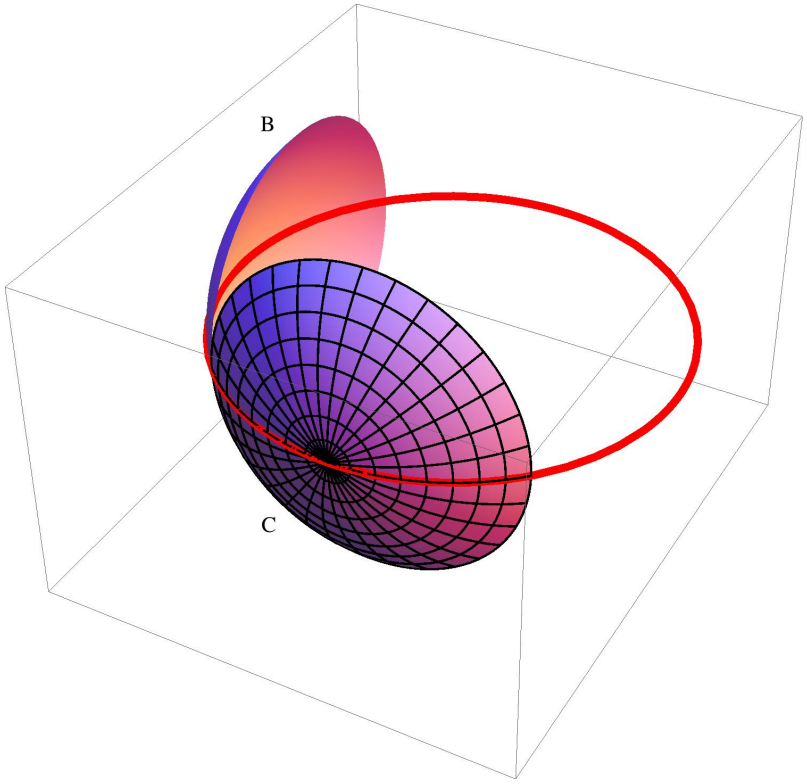

Figure S11: Hidden surface. Light entering the branch cut of three-dimensional electromagnetic space (Fig. S8) propagates along circles that are the images of the great circles on the hypersphere in stereographic projection. The light that has entered through the branch cut C cannot cross the surface B but at most skim along it, because B is part of the two-dimensional equatorial sphere of the hypersphere. The red circle shows an example: a light ray skimming along the surface B. Since light never crosses B, one can inflate it like a balloon to make space for the hidden interior of the invisibility device.

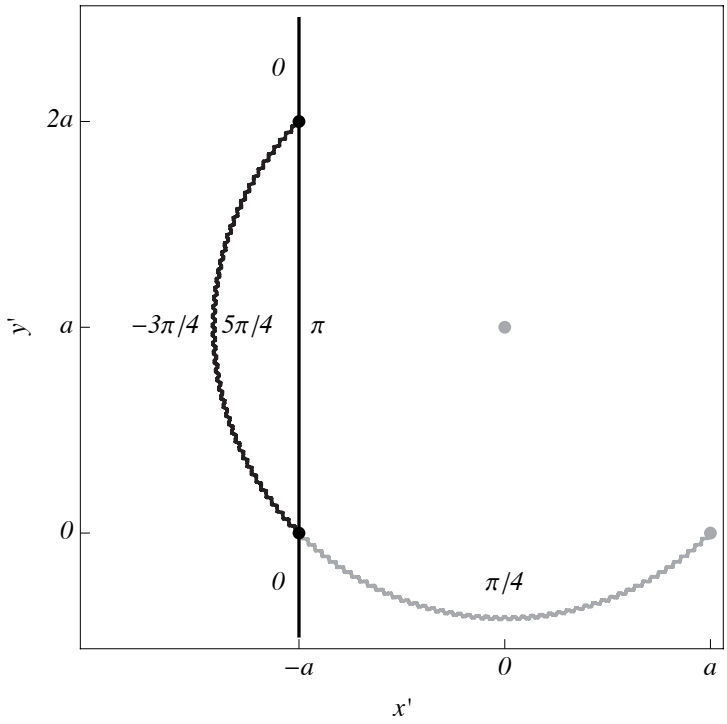

Figure S12: Creating a hidden space in three dimensions. The diagram shows the intersection of the branch cuts in electromagnetic space (Fig. S11) with the plane at $z' = 0$. Light enters the non-Euclidean branch through the zigzag line indicated in gray, the first branch cut. The gray dot at $(0, a)$ indicates the stereographic projection of the south pole of the hypersphere, the center of Maxwell's Fish Eye. The second branch cut, shown in black, is to be inflated in a similar way as the first one has been expanded to create $\{x', y', z'\}$ space. This second expansion of space is described in toroidal coordinates with the branch points as poles, indicated in black. In these coordinates, the first branch cut corresponds to a bipolar angle of $\sigma_1' = \pi/4$ and the second branch cut to $\sigma_1' = -3\pi/4$ and, equivalently, $\sigma_1' = 5\pi/4$. The $5\pi/4$ side of the branch cut is deformed to the plane segment at $\sigma_1' = \pi$ while the $-3\pi/4$ side is opened to ∞ to form the other plane segments at $\sigma_1' = 0$ that, together with the first segment, constitute the entire plane $z' = -a$, indicated as a black line in the figure. In this way, the "interior" of the inflated branch cut has been expanded to the half of $\{x', y', z'\}$ space left of the plane $z' = -a$. This region corresponds to the invisible interior of the cloaking device that appears, after the required coordinate transformation to physical space, as the lentil-shaped object in Fig. 3 of our paper.

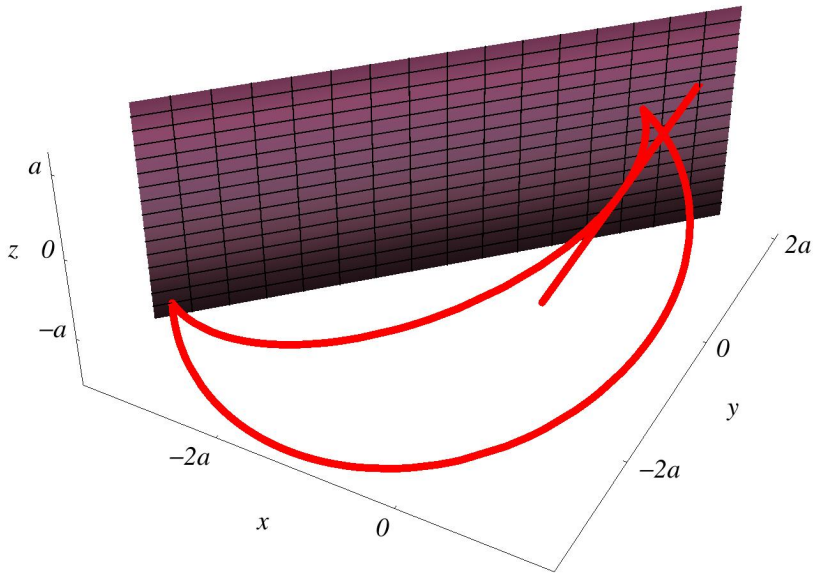

Figure S13: Hiding behind a mirror in three-dimensional electromagnetic space. The figure shows the trajectory of a light ray in both branches of electromagnetic space. In the Euclidean branch the ray follows a straight line. Then the ray enters the non-Euclidean branch where it is bent, following the stereographic projection of a great circle in hyperspace, which is a circle in three dimensions. The ray hits the mirror and is reflected. The reflected ray continues on the reflected great circle, the mirror image of the light trajectory without the mirror. After another reflection the ray is back on the original path. It leaves the branch cut in the same direction as it has entered, irrespective of the detour in non-Euclidean space. In this way the space behind the mirror is hidden and the act of hiding does not appear on light rays.

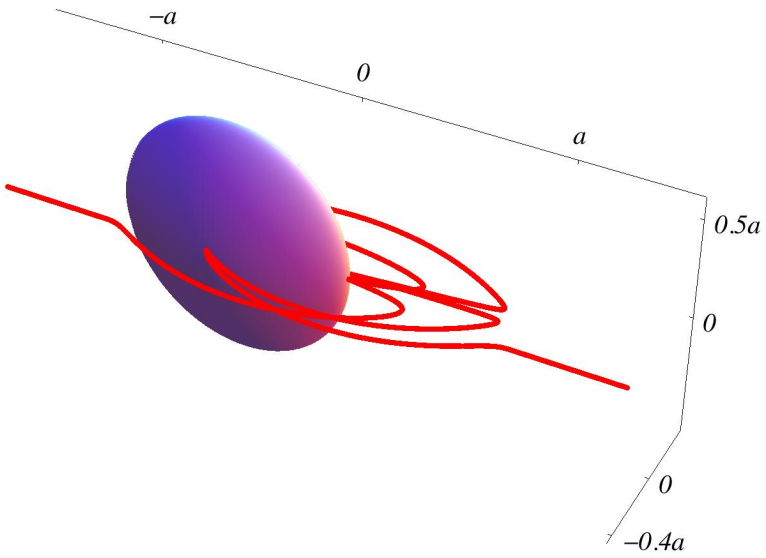

Figure S14: Hiding behind a mirror in three-dimensions, ray tracing. The figure displays the trajectory of a light ray in physical space. It shows a case where the ray performs two loops in the non-Euclidean branch of electromagnetic space, similar to Fig. 3B of our paper. The ray is reflected four times at the mirror (one reflection is shown in front), but leaves the device as if it would have travelled through empty space.

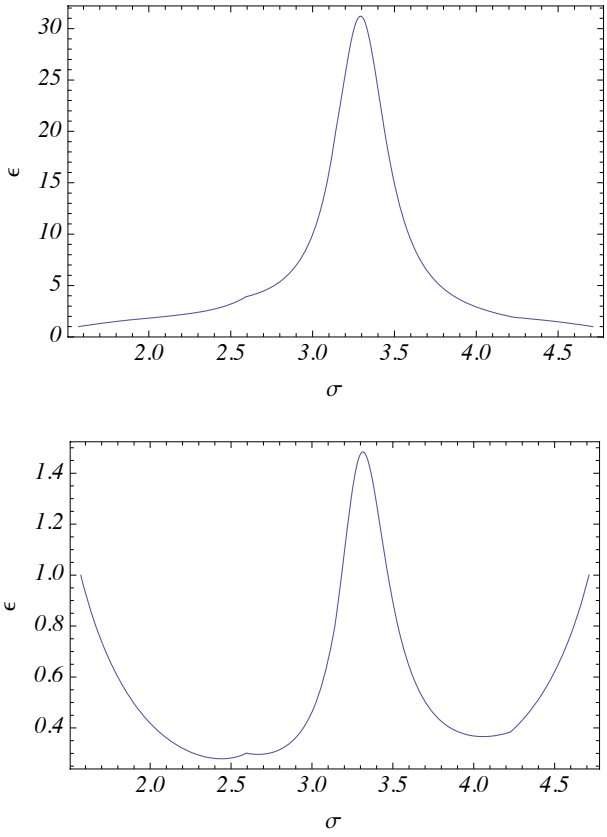

Figure S15: Electric permittivity ε as a function of the toroidal angle σ in physical space. We put $\tau = 0$, because ε is extremal here. We focus on the range of space occupied by the invisibility device and plot the curves for σ running from $\pi/2$ to the boundary of the device at $3\pi/2$. Top: curve for the polarization where ε reaches a maximum. Bottom: curve where ε becomes minimal.